

Visual Analysis of Defects in Glass Fiber Reinforced Polymers for 4DCT Interrupted *In situ* Tests

Alexander Amirkhanov¹, Artem Amirkhanov¹, Dietmar Salaberger¹, Johann Kastner¹, M. Eduard Gröller^{2,3}, Christoph Heinzl¹

¹University of Applied Sciences Upper Austria, Campus Wels, Austria

²Institute of Computer Graphics and Algorithms, Vienna University of Technology, Austria

³VRVis Research Center, Austria

Abstract

Material engineers use interrupted *in situ* tensile testing to investigate the damage mechanisms in composite materials. For each subsequent scan, the load is incrementally increased until the specimen is completely fractured. During the interrupted *in situ* testing of glass fiber reinforced polymers (GFRPs) defects of four types are expected to appear: matrix fracture, fiber/matrix debonding, fiber pull-out, and fiber fracture. There is a growing demand for the detection and analysis of these defects among the material engineers. In this paper, we present a novel workflow for the detection, classification, and visual analysis of defects in GFRPs using interrupted *in situ* tensile tests in combination with X-ray Computed Tomography. The workflow is based on the automatic extraction of defects and fibers. We introduce the automatic Defect Classifier assigning the most suitable type to each defect based on its geometrical features. We present a visual analysis system that integrates four visualization methods: 1) the Defect Viewer highlights defects with visually encoded type in the context of the original CT image, 2) the Defect Density Maps provide an overview of the defect distributions according to type in 2D and 3D, 3) the Final Fracture Surface estimates the material fracture's location and displays it as a 3D surface, 4) the 3D Magic Lens enables interactive exploration by combining detailed visualizations in the region of interest with overview visualizations as context. In collaboration with material engineers, we evaluate our solution and demonstrate its practical applicability.

Categories and Subject Descriptors (according to ACM CCS): Image processing and computer vision [I.4.7]: Feature Measurement—Life Cycle; Image processing and computer vision [I.4.10]: Image Representation—; Computer graphics [I.3.0]: General—

1. Introduction

Currently, composite materials attract a lot of interest from industry. Utilizing glass fiber reinforced polymers (GFRPs) enables the manufacture of cost-effective products with tailored mechanical properties. GFRPs consist of two components: glass fibers and a polymer matrix. Glass fibers provide the material with stiffness and durability. The polymer matrix bonds the fibers, protects them from external damage, and provides resiliency to the material. In order to achieve improved material strength, the fibers are oriented during the manufacturing process. Low weight and high durability of GFRPs make them especially suitable for production in areas such as the aerospace and automotive industries. In order to produce GFRPs that satisfy industrial requirements, material engineers are highly interested in finding and analyzing the correlations between material features (e.g., the number of fibers, their directions and diameters, etc.) and the resulting mechanical properties, such as strength and ability to withstand high loads. This research knowledge is then utilized for optimizing the manufacturing process to produce superior composite materials.

3D X-ray Computed Tomography (3DCT) is an inspection method that is widely used for the non-destructive testing of composite materials such as GFRPs. Typical 3DCT scanners comprise three major components: X-ray tube, rotary plate, and detector. The inspected specimen is placed on the rotary plate between the tube and the detector, whereupon the scanning process starts. The X-ray tube directs X-rays through the specimen and onto the detector. The detector registers a 2D X-ray attenuation image also called projection image. The rotary plate is then turned and the process is repeated until a full 360° rotation of the specimen is completed. Tomographic reconstruction is performed using the set of 2D projection images to produce a 3D (volumetric) attenuation image. 3DCT has two main advantages over other non-destructive methods: 1) it allows the user to explore all internal and external structures with just one scan, and 2) it provides a high imaging resolution capable of resolving individual fibers and small defects. However, 3DCT cannot be directly used for the inspection of the specimen under various loads. The specimen has to be static during the scanning procedure, which can last up to several hours. To circumvent this limitation, interrupted *in situ* tensile 3DCT tests can be used.

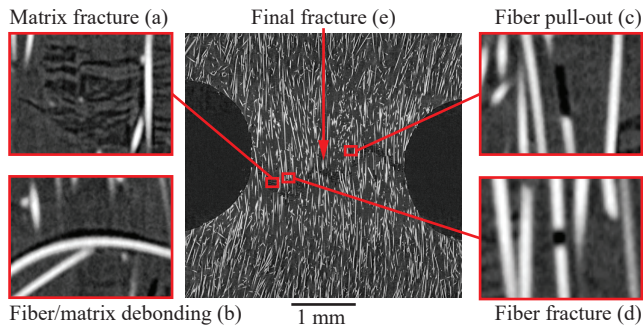


Figure 1: Four defect types on a 2D slice of a 3DCT volume coming from an interrupted *in situ* tensile test.

Material engineers rely on interrupted *in situ* tensile testing to study on the damage mechanisms in composite materials. During interrupted *in situ* tensile testing, a specimen is scanned under various loads created by the loading tensile stage. Typically, the first scan is performed without any load. For each subsequent scan, the load is incremented until the specimen is completely fractured. The series of 3DCT scans will henceforth be referred as 4DCT data, where the fourth dimension is the time or the amount of force applied to the specimen during the scan. If interrupted *in situ* testing is performed, defects of four types are expected to appear in the GFRPs: matrix fractures, matrix/fiber debondings, fiber pull-outs, and fiber fractures (see figure 1). Detection, classification, and visualization of these defects is of a high interest for material engineers. Klaus Friedrich described and illustrated each defect type (failure mechanism) [FRI89]. However, the provided description does not formalize differences between defect types to an extent that is sufficient for an automatic defect classification. Therefore, in collaboration with our industrial partner Borealis AG, a major supplier of plastic materials for engineering applications in the automotive industry, we further detailed the defects' description. It resulted in the following list of definitions for each defect type:

- **Matrix fractures** are mostly perpendicular to the force direction. They are often clustered and their shapes do not correlate with any shapes of fibers in the proximity (see figure 1a).
- **Fiber/matrix debondings** mostly affect fibers that are perpendicular to the force direction. They occur above or below fibers. Debondings have directions and shapes similar to neighboring fibers (see figure 1b).
- **Fiber pull-outs** mostly affect fibers that are aligned parallel to the force direction. They only occur at the ends of fibers and are cylindrical in shape. Diameter and direction of a pull-out are the same as those of the corresponding fiber (see figure 1c).
- **Fiber fractures** are located between two fiber pieces. They have a cylindrical shape. The fracture diameter is approximately equal to the fiber diameter (see figure 1d).

If a force is applied, which is larger than a test specimen can sustain, individual defects of different types accumulate and the *final fracture* is formed as a result. The final fracture runs through the specimen and separates it into two parts (see figure 1e).

In this work, we investigate the Fibremod GD301 material pro-

duced by Borealis AG. This material is glass fiber reinforced polypropylene with a fiber in weight content of 30%. Due to its strong mechanical qualities this material is used in air bag housings, pedal carriers, pump housings, etc. During interrupted *in situ* tensile testing, a force inducing stress, strain, and failure was applied to the material. The material's failure is caused due to numerous individual defects that can be classified into the four previously mentioned types.

In section 2 we proceed by deriving seven tasks that are important for the 4DCT analysis and present a workflow for solving these tasks. In section 3 we provide a literature overview and discuss the related work. In section 4 we give a detailed description of the datasets used in this work. Sections 5 and 6 describe the workflow in greater details, that is, defect classification and tools for visualization and analysis are presented. In section 7 we apply the proposed system and present use cases. We discuss the design choices made when implementing the presented visualization and analysis methods in section 9. In section 10 we provide conclusions.

2. Workflow and Task Analysis

Interrupted *in situ* tensile testing in combination with 3DCT is a relatively novel topic. Currently commercial available software such as VGStudio Max [VGS] or Avizo 3D [Avi] provide a wide range of functionalities such as segmentation, surface determination, feature extraction, porosity/inclusion analysis, and fiber analysis. However, the functionalities are not sufficient for 4DCT data analysis and do not cover the requirements of our domain specialists. To the authors' knowledge, there is no tool currently available that can extract and classify defects from tensile tests of GFRPs and perform a visual analysis of these defects on the 4DCT data.

In the course of this project, we collaborated with a major supplier of plastic materials for engineering applications in the automotive industry: Borealis AG. They aim to use the 4DCT tensile test data analysis to acquire new knowledge and insights on the correlation between fiber characteristics and resulting material properties. This knowledge is then used to improve the in-house fiber simulation software. In particular, the dynamics of defect development under the load is of high interest. After several meetings and discussions, we identified the following list of tasks, which are of highest relevance for analyzing 4DCT data, and cannot be automatically implemented with existing software:

- T1:** Finding individual defects and calculating defect characteristics, such as size, the center of mass, and direction.
- T2:** Classification of each individual defect by type.
- T3:** Visualization of individual defects.
- T4:** Finding and visualizing regions with the highest defect densities.
- T5:** Finding and visualizing the final fracture that appears when the specimen is completely fractured.
- T6:** Visualizing the history of the material destruction under the influence of increasing load.
- T7:** Presenting quantitative information on the final fracture and defects.

The purpose of the work presented here is to overcome the limitations of existing analysis techniques and to present a workflow

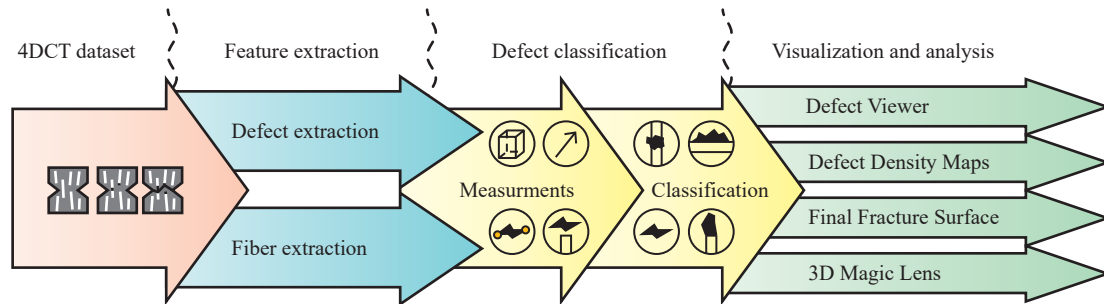


Figure 2: An overview of the workflow for 4DCT interrupted in situ tensile-test data-analysis.

and a system that address the tasks listed above. An overview of the workflow is shown in figure 2.

Defect and fiber extraction: The first stage of the workflow is to extract individual defects and fibers (T1). For the defect segmentation, we use binary thresholding on the data that is pre-filtered with gradient anisotropic diffusion to reduce noise. For the fiber extraction, we employ the algorithm proposed by Salaberger et al. [SKK*11].

Defect classification: To classify defects (T1, T2), we introduce an automatic defect classifier based on the assumptions we made together with material engineers. Using these assumptions, a type is assigned to each defect in a 4DCT dataset. The complete list of assumptions for each type concerning defect characteristics as well as the details of classification process are provided in section 5.

Visualization and analysis: As the last stage of the workflow, we present a visual analysis system that provides a set of visualization techniques that aim to address tasks T3 – T7. A detailed description is given in section 6. The system comprises four different visualization methods that can be combined or used sequentially to achieve the analysis goals:

- The *Defect Viewer* (section 6.1) highlights defects (T3) in 2D slices of the CT data and provides visual encodings for the various defect types.
- The *Defect Density Maps* (section 6.2) encode the defect distributions by type and provide visualizations of these distributions in 2D and in 3D (T4). In addition, Defect Density Maps provide quantitative information on the frequency of defect occurrences in a region (T7).
- The *Final Fracture Surface* (section 6.3) estimates the shape and location of a final fracture as a 3D surface and displays it on top of the contextual information in a 3D view (T5).
- The *3D Magic Lens* (section 6.4) is an interactive tool facilitating the analysis by combining detailed visualizations in the region of interest with overview visualizations as context in a single 3D scene. In addition, displaying data from different time-steps in the same scene is possible (T6).

3. Related Work

Visualization of 3DCT data: One of the first works utilizing visualization techniques for non-destructive testing using industrial 3DCT data was done by Huang et al. [HMMW03]. The authors focused on feature extraction and visualized the data using direct

volume rendering with two-dimensional transfer functions. Heinzl et al. [HKG07] introduced a method for surface extraction from multi-material components using dual energy CT. Hadwiger et al. [HLRS*08] presented a method for analyzing 3DCT data with the goal of interactively detecting, classifying, and quantifying features using a visualization-driven approach. The work by Fritz et al. [FHG*09] focused on characterizing steel fiber-reinforced concrete by segmenting fibers and quantifying their properties. A direction-sphere histogram provided an overview of the fiber orientations. Direction transfer functions defined to encode orientations are used to color-code fibers. More recent publications addressed the visualization of carbon- and glass-fiber reinforced composites using 3DCT scans. Weissenböck et al. [WAL*14] presented the FiberScout tool for exploring and analyzing carbon fiber reinforced polymers. The authors used 2D information visualization methods, such as parallel coordinates, coupled with a scatter plot matrix as well as 3D visualization techniques, such as blob surfaces and metadata visualization. Within the same framework Reh et al. [RGK*13] implemented the mean object (MObject) technique for analyzing pores in carbon fiber reinforced polymers. The MObject technique was used for the exploration of hierarchically clustered pores and the identification of common patterns in the pore shapes.

Visualization of time-varying data: Havre et al. [HHN00] presented the ThemeRiver approach for visualizing thematic variations over time within a large collection of documents. The work by Silver et al. [SW97] focused on tracking and visualizing features in computational fluid dynamics datasets. The authors extract features from each individual step and use spatial overlap to determine matching. Feature properties and their evolution history are used to enhance isosurface visualization and volume rendering. Van Pelt et al. [vPOBB*10] presented a framework for analyzing blood-flow dynamics and visualizing essential characteristics.

Segmentation and extraction of features and defects: Zhou et al. [ZYZ10] used images from a camera that is fixed on a vehicle for the analysis of an asphalt canvas. The authors presented an illumination-invariant image-enhancement and segmentation algorithm for the extraction and classification of pavement cracks. Several approaches have been presented for an automatic crack detection in industrial 3DCT data. The work by Landstrom et al. [LT12] focused on crack detection in steel slabs. The authors presented an automated on-line system, based on 3D profile data of steel slab surfaces, which utilizes morphological image processing

and statistical classification by logistic regression. Yamaguchi et al. [YNH08] proposed an efficient and high-speed method for automatic crack detection on concrete surfaces employing percolation-based image processing. In civil engineering, the corrosion of steel reinforcements in structural elements of concrete bears the risk of reduced stability. The work by Paetsch et al. [PBP*15] explored various image processing and visualization methods for 3D corrosion detection in time-dependent 3DCT images of concrete. Specimens are exposed to several cycles of electrochemical pre-damaging to generate a large artificial crack. Bhowmik et al. [BMH*14] introduced a method for the detection and segmentation of cracks from 2D cross-sectional images of rock under compressive force. A two-dimensional matched filtering technique is followed by local entropy-based thresholding, morphological operators, and length filtering.

All the works as mentioned above focused on a single type of defect and usage scenario. In these works, 3D or even only 2D datasets are processed. 4DCT data is considered in the work of Paetsch et al. [PBP*15] and is visualized using side-by-side views. Reh et al. [RAK*15] presented a tool for evaluating 4DCT data. A tracking graph [WCBP12] was employed to relate pores in a specimen between scans. The system we are proposing provides means for the extraction and classification of four different defect types (matrix fractures, fiber pull-outs, debondings, and fractures) and methods for the detailed integrated visual analysis of these defects.

Various image segmentation methods are employed in medical and industrial 3DCT for feature detection and classification. These methods range from simple or automatic thresholding methods, e.g., Otsu thresholding [Ots79], to more popular probabilistic methods, such as random walks [Gra06]. The visual analysis in our proposed system is not limited to a particular image segmentation algorithm. Our flexible system allows users to apply any segmentation algorithm for defect detection. The system we are proposing determines fibers using an algorithm presented by Salaberger et al. [SKK*11], which is designed for individual fiber extraction in fiber-reinforced composite materials.

4. Data Description

We performed series of measurements under load of three test specimens on a GE phoenix|xray nanotom® device. The corresponding 3DCT scans contain three components with different gray-value ranges (from high to low): fibers, matrix, and air.

Dataset 1: The specimen is notched in order to ensure failure in a predefined region. This is important, as high resolution 3DCT scanning with high magnification is only possible if the scan volume is reduced to a particular region of the test object. The force direction and the main fiber orientation are parallel, which leads to characteristic failure modes. It is expected that fiber pull-outs occur more frequently than fiber/matrix debondings. Four scans of a GD301-MiniNotched-OH1 object were performed with 0, 208, 224, 244, and 260 newton of force applied. The voxel size is 2 μm .

Dataset 2: This specimen is notched as well, the main fiber orientation and the force direction are perpendicular. Therefore, it is expected that fiber/matrix debondings will occur more frequently than fiber pull-outs. The scans were performed with 0, 187, 212, 225, 230, and 235 newton. The voxel size is 2 μm .

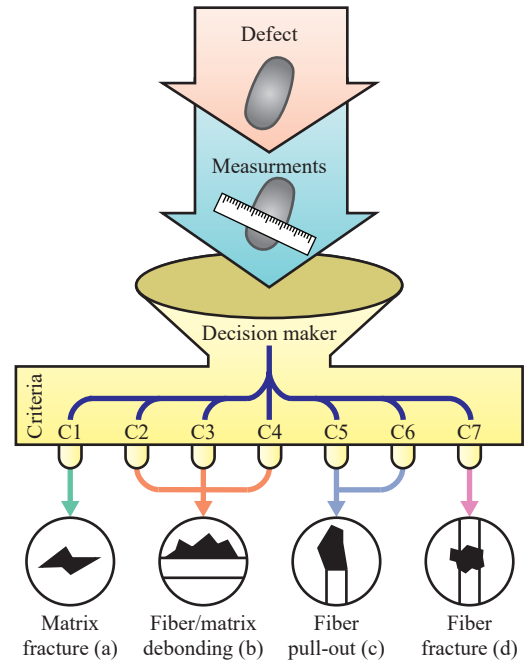


Figure 3: The pipeline for measurement and classification of individual defects. Defect types are assigned based on the combination of criteria C1-C7 that are evaluated: C1 - matrix fracture (a), C2, C3, C4 - fiber/matrix debonding (b), C5, C6 - fiber pull-out (c), and C7 - fiber fracture (d).

Dataset 3: The specimen is narrowed in the middle and extended at the ends. Similarly as for the notched specimens, this narrowed geometry guarantees that the failure happens in a predefined region. However, in this case the expected defect region is rather large in comparison to notched specimens. In our dataset, the final fracture occurs on the top of the scanned region. The scans were performed with 0, 374, 396, 405, 414, 422, 431, 440, and 449 newton. The voxel size is 3 μm .

5. Defect Classifier

The Defect Classifier takes labeled images of defects and extracted fibers as inputs (see figure 2). An automatic defect classification is then performed in two steps. In the first step, we measure geometrical features of the defects. In the second step, we assign the most suitable type to each defect based on the measured features (see figure 3).

Measuring geometrical features of defects: For each defect the following characteristics are measured: 1) length, width, depth; 2) direction; 3) volume (as the sum of a defect's voxel volumes); 4) position; and 5) existence of neighboring fibers (see figure 4). We use the LabelGeometryImageFilter as provided by the Image Segmentation and Registration Toolkit (ITK) [ITK] to derive these geometrical characteristics. In addition, for each defect an object-oriented bounding box (OOBB) is computed. In order to determine the OOBB, the voxels of a defect are analyzed. The 3D positions of the voxel centers are used as data points for a principal compo-

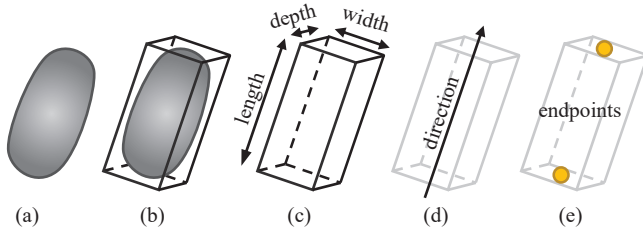


Figure 4: Characteristics important for the defect classification: the original defect shape (a); object oriented bounding box (b); length, width, and depth (c); direction (d); endpoints (e).

nant analysis (PCA). PCA produces an orthogonal basis of three eigenvectors from the covariance-matrix, which are taken as the OOB axes. The eigenvector with the largest eigenvalue indicates length, the second largest eigenvalue indicates width, and the smallest eigenvalue indicates depth (see figure 4). To calculate the exact extent of the OOB, the voxel centers are projected onto the eigenvectors and min-max ranges are determined for each vector.

Assigning the defect type: To assign the most appropriate type to each defect we introduce a detailed list of criteria for each defect type. The derivation and formalization of these criteria were performed by material engineers from Borealis AG, who provided us with criteria for defect classification commonly accepted in industry. Recently, work by Rolland et al. [RSR15] used a similar system of criteria for classifying defects in glass-fiber-reinforced thermoplastics. The resulting criteria (C1-C7) for the defect types are as follows:

Matrix fracture:

C1: The angle between the matrix fracture direction and the force direction is more than 25° .

Fiber/matrix debonding:

C2: The angle between the debonding direction and the force is more than 45° .

C3: The ratio between the width of a debonding and its depth should be in the range [0.5, 2].

C4: The ratio between the length of a debonding and its width should be larger than 4.

Fiber pull-out:

C5: The angle between the fiber pull-out direction and the force direction is less than 25° .

C6: In close proximity of a *fiber pull-out* there has to be at least one fiber end. The angle between the defect direction and the fiber direction has to be less than 10° .

Fiber fracture:

C7: In close proximity of a *fiber fracture* there have to be at least two fiber ends. The defect has to be in between these fibers.

A classification is assigned to a potential defect if respective conditions are satisfied. The connected component ID of the defect is then added to the defect-type list. There are four lists in total. It is possible that a defect is assigned to more than one classification, in which case the defect ID is stored in multiple lists.

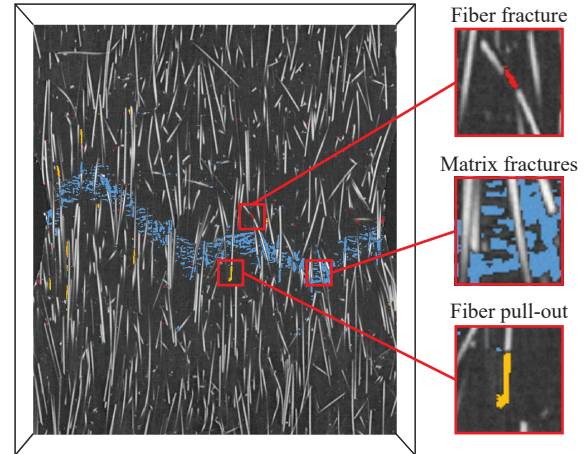


Figure 5: The Defect Viewer shows the original image of Dataset 1 as context with highlighted fiber pull-outs, matrix fractures, and fiber fractures.

6. Visualization and Analysis

The visual analysis system integrates a set of techniques for investigating the 4DCT data of interrupted *in situ* tests. The techniques can be used separately or combined in a single 3D scene. To initiate a visualization method, the user specifies the required files, which are stored in a resource manager. The resource manager keeps links to all files involved in the analysis and loads them automatically on demand. Each visualization method can then be added or removed from the 3D scene setup, which allows the user to build visualizations tailored to the current analysis goal. A goal could be for example comparing different stages of the tensile test, comparing distributions of defects by type or by region, getting an overview or detailed visualizations of defects, and interactive exploration.

6.1. Defect Viewer

The Defect Viewer displays a 3DCT dataset in 2D slices. Defects in these slices are highlighted according to their type (see figure 5). The user can change the slice position and orientation. To perform defect highlighting, a labeled image and a list of defects are required. The user-specified colors are assigned to defects of the different types. The image containing the 2D slice with defect highlighting is computed on-the-fly. This Defect Viewer can provide the context in case it is combined with other visualizations.

6.2. Defect Density Maps

One of the features of the visual analysis system is calculating and visualizing Defect Density Maps. Defect Density Maps can be calculated for particular defect types or for all defects. They provide an overview of the distribution of defects by type and help to visually determine regions with the highest number of defect occurrences. A general overview of the material is provided, which enables decision making based on defect-density and fiber-characteristics distributions in the areas of interest. Figure 6 illustrates Defect Density Maps of fiber pull-outs (a), matrix fractures (b), fiber fractures (c),

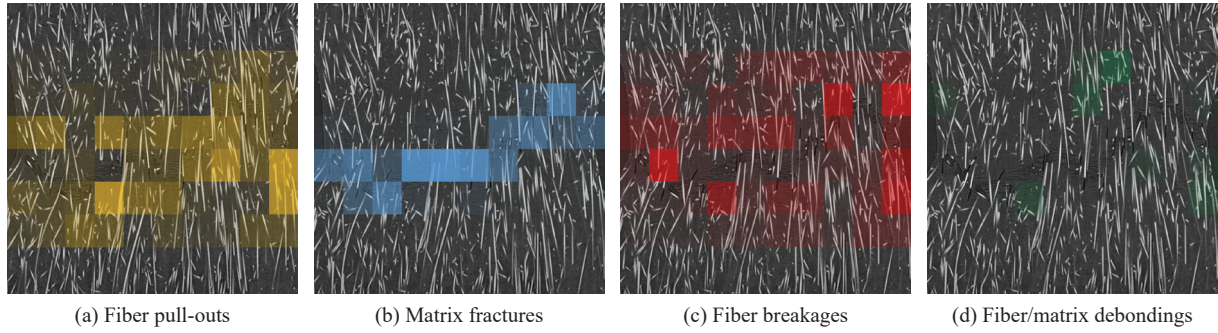


Figure 6: Four Defect Density Maps displaying distributions of fiber pull-outs (a), matrix fractures (b), fiber breakages (c), and fiber/matrix debondings (d) in Dataset 1.

and fiber/matrix debondings (d). The distribution of defects depends on the defect type. Matrix cracks mostly occur in the region of the final fracture, while fiber pull-outs and fiber fractures occur close to the final fracture region. Material engineers use density maps to correlate fiber characteristics with defect occurrences, e.g., correlation of fiber pull-outs to fiber orientation. Defect Density Maps can be visualized in 2D slices or in 3D view directly using smooth surfaces.

Defect Density Maps calculation: A Defect Density Map is generated from the labeled image and the list of defects. From the labeled image, a mask of defects is extracted. The mask is then divided into subregions. For each subregion, the number of voxels belonging to defects is calculated and stored in a Defect Density Map.

2D visualization: A color transfer function assigned to the density map allows users to identify areas with a specific rate of defect occurrence. Finally, the density map is superimposed on the original CT data in the Defect Viewer using an opacity transfer function, where opacity increases proportionally to density.

3D visualization: Defect Density Maps in 3D can be represented by smooth semi-transparent isosurfaces with contours around areas of interest (areas with high defect densities) (see figure 7). Alternatively, the direct volume rendering using color and opacity transfer functions can be employed (for example, see figure 11). The iso-surfaces are calculated from the Defect Density Map by marching-cubes surface-extraction using a user-specified threshold value. As a result, the surfaces are calculated for regions where the defect density is higher than the threshold. Gaussian blurring can be applied to smooth the region surfaces. Multiple surfaces can be extracted for any combination of tensile-test stage and defect type. Colors of the surfaces are configurable. 3D Defect Density Maps can be used for comparing defect distributions of different types in one stage or for comparing distributions of a given defect type for several or all tensile-test stages (see figure 7 and figure 9). This visualization facilitates the exploration of the defect-development process in the material as the load increases.

6.3. Final Fracture Surface

The shape of the final fracture provides relevant information about specimen's mechanical properties. The final fracture always occurs in the weakest region of the specimen. The fracture shape, there-

fore, serves as an important indicator of the material properties. The main challenge in the analysis of the final fracture is to properly define its shape. Figure 8 shows the final fractures for Datasets 1, 2, and 3. The final fracture first occurs at a force of 244 newton. At a force of 260 newton, the final fracture widens while preserving the shape.

Calculation: The surface is constructed such that it runs through the middle of the final fracture in the direction of the applied force (see figure 10). The fracture-surface extraction is performed as follows: Rays are cast along the force direction (usually from top to bottom) through the segmentation mask of a fracture. One ray is cast for each column of voxels. The ray starts at the center of a top voxel and ends at the center of the corresponding bottom voxel. For each ray the average position of all fracture voxels along the ray is then determined (see figure 10). Finally, for all rays these positions correspond to points on the fracture surface. A Gaussian filter can

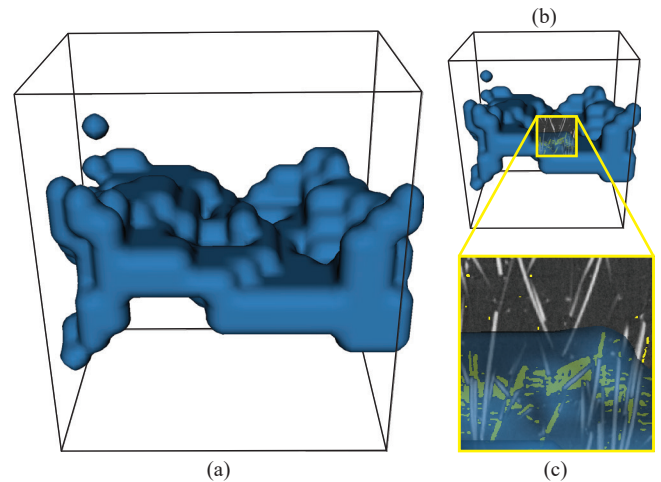


Figure 7: The Defect Density Map isosurface outlines the high-defect density region in 3D for Dataset 1 (a). A slice with defects highlighted in yellow is shown using the 3D Magic Lens (b). A zoom-in into the region of interest demonstrates that the isosurface efficiently separates regions containing high amount of defects (c).

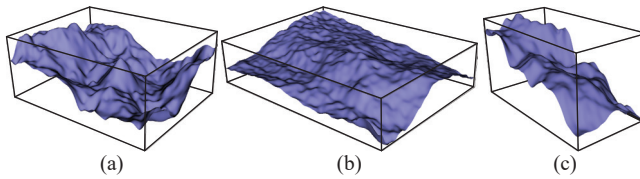


Figure 8: The Final Fracture Surfaces show differences between the final fractures of Datasets 1 (a), 2 (b), and 3 (c). Dataset 2 has the fracture surface that is flatter than for Datasets 2 and 3.

then be used to reduce noise and smooth the surface, which can be then stored as a height map.

6.4. 3D Magic Lens

To combine different visualization techniques together we implemented a 3D Magic Lens. The 3D Magic Lens is an interactive tool that changes the object appearance in a selected region (see figure 9). Any possible combinations of available visualization methods and test stages can be chosen for the selected region and for the surrounding area. This is achieved by rendering 3D scenes twice from the same camera position and then displaying a part of one image on top of the other one. The 3D Magic Lens has a rectangular shape and the user can change its position and size. We assume three usage scenarios of the 3D Magic Lens:

1. Analyzing and comparing differences between tensile test stages. For instance, it is possible to use an early stage of the test for providing the context, while studying defects at a later stage within the region of interest. The usage example is given in figure 9a.
2. Applying a specific combination of visualization techniques in the region of interest. For example, figure 9a demonstrates that with the 3D Magic Lens the user can interactively enable defect highlighting with the Defect Viewer in a small region; in figure 9b the Defect Density Map of all defects provides the context, while the Density Maps of individual defects are shown in the region of interest.
3. Looking through the occluding visualizations such as Density Maps by disabling them in the region of interest. This enables an interactive visual analysis, where the overview is provided with one set of techniques, and details are shown with other set of visualizations. The usage example is given in figure 9c.

The 3D Magic Lens visualization can be used in two modes: a side-by-side mode (figure 9a), and a conventional magic lens mode (figure 9b,c).

7. Evaluation and Results

From the beginning of this work, we closely collaborated with material engineers from the industrial company Borealis AG. The company is focused on the production of polyolefins. During our collaboration, Borealis AG provided us with test specimens, which are made of the Fibremod GD301 material. Our goal was to create approaches for analyzing 4DCT data and to develop a tool, which implements these approaches. The tool was developed for and is

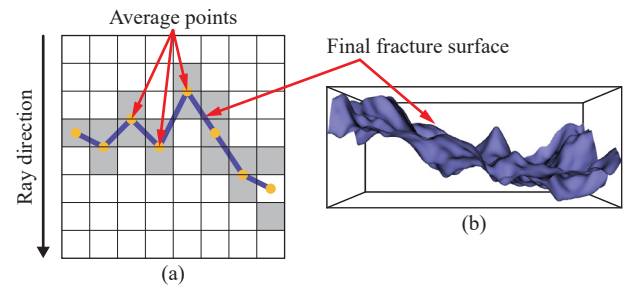


Figure 10: To calculate the Final Fracture Surface rays are casted from top to bottom. An average position of defects is calculated for each ray (a). The resulting height-map is then smoothed and reconstructed into a 3D mesh (b).

mainly used by material engineers of UASUA. At the beginning of the project, we had several meetings with material engineers. During these meetings we identified and specified the analysis tasks given in section 2. We then aimed to support the tasks with our approaches. We regularly had internal meetings with the material engineers of UASUA. During these meetings, we discussed new ideas and refined existing ones. We started from initial ideas and iteratively improved and developed them while staying in a close feedback loop with the users. If we required additional input, we contacted Borealis AG and discussed the open topics. For example, we learned that all the four defect types are interesting to the material engineers and there are no types, which we could ignore. In addition, we discussed where the transition limits between defects types are (e.g., when a fiber pull-out becomes a matrix fracture). Together with the partner, we frequently assessed the correctness of our assumptions. In addition, we regularly demonstrated our approaches and results. We got a positive feedback concerning results of the Defect Classifier tool. They were very much interested in the automatic defect classification and found the tool as very useful concerning the description of the fracture mechanism. The utility of the Density Viewer tool was estimated highly as well. In the Defect Density Maps, they appreciated that it highlighted regions of a high density and enables finding correlations between internal material characteristics and these regions. In the 3D version of the Density Maps they liked that it can provide a description of the material destruction process with a visualization technique that is easy to interpret. Material engineers also appreciated the ability to quickly compare different 4DCT datasets as well as different stages of a single tensile test with each other.

Additionally, we interviewed a material engineer at UASUA who is one of the main users of our software. We asked about the software usability and the usefulness of the developed tools, and whether they met the defined goals. In general, the user appreciates that the approach with a single 3D scene is interesting and agile. Regarding the individual visualization tools, we have got the following feedback:

Defect Classifier: Similar to the material engineers from Borealis AG we got a positive feedback about the tool. The interviewee thought that the provided defect extraction and classification provides important information for the 4DCT analysis.

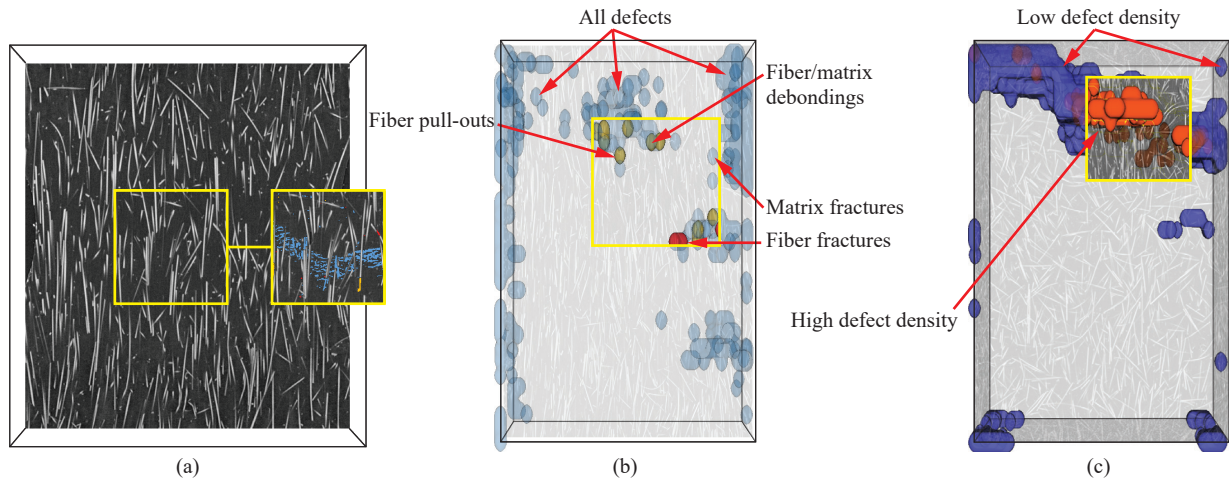


Figure 9: The usage scenarios of the 3D Magic Lens: (a) Comparing two stages (244 N and 260 N) of Dataset 2 in the side-by-side mode. Defects are highlighted for the 260 N stage. (b) Comparing a Defect Density Map of all defects to the Density Maps for matrix fractures (blue), fiber/matrix debondings (green), fiber pull-outs (yellow), and fiber fractures (red). The 440 N stage of Dataset 3 is used. (c) Exploring the Density Map isosurface with high density (red) together with the 2D slice of CT data in the context of isosurface with low density (blue).

Defect Viewer: The material engineer's opinion is that the Defect Viewer's concept fits well into the visualization the toolbox. The tool integrates well into the 3D scene and is well suited for combining and interacting with other tools in the toolbox.

Defect Density Maps: The value of this tool was evaluated as high. The material engineer felt that Defect Density Maps help in gaining important information about the defects' distribution as well as finding a correspondence between internal characteristics and the damage (final fracture shape and the number of defects close to it).

Final Fracture Surface: The material engineer appreciated "a nice overview of the fracture" that this tool provides. He also mentioned that the possibility of measuring the distance between the highest and the lowest points would be of use to him.

3D Magic Lens: The tool was highly commended due to its flexibility and ability to supplement many other tools in solving a number of tasks. The interviewee appreciated that the interactive comparative visualizations provided by the 3D Magic Lens allowed him to observe and analyze the fracture evolution.

8. Use cases

Use case 1: Using the Final Fracture Surface a material engineer compared fractures of specimens with different major fiber orientations, i.e., 0° orientation (Datasets 1 and 3) and 90° orientation (Dataset 2). Before the fracture extraction, material engineers assumed that the specimen with the 90° fiber orientation will have the flattest fracture surface of all three. The visualization results provided by the Final Fracture Surface confirmed this assumption (see figure 10). The results show that the 0° fiber orientation fracture has higher peaks, more variance, and a larger distance between the maximum and minimum points.

Use case 2: To evaluate defect distributions the users have built

density maps for defects of each type (see figure 6). The visualizations clearly show that matrix fractures are located mostly in the region of the final fracture while fiber pull-outs and fiber fractures are distributed in a wider region. However, a more detailed analysis using the Defect Viewer and the 3D Magic Lens tools revealed that all defects contributed to the development of the final fracture. The fracture developed in the areas with the highest densities of matrix fractures, while several fibers adjacent to the final fracture had fiber fractures and fiber pull-outs on both ends. As fiber pull-outs often occur at the fiber ends that point away from the final fracture, fiber pull-outs are characterized by a wider distribution.

Use case 3: First, to get an overview, the user compares density maps of all defect types for all the stages of the tensile test (figure 11). It can be seen that the 440 N stage is of high importance: defects accumulate critical mass before the final crack is formed. The user then chooses to investigate this stage in more detail using the 3D Magic Lens by visualizing distributions of individual defects in the context of the total defect density (figure 9b). It can be seen that there are many fiber/matrix debondings and matrix cracks in the center of the top area. Therefore, this is the weakest region, where the final crack will appear. Finally, the user applies the 3D Magic Lens showing areas with the highest defect density in the context of the CT data to study individual defects in the weakest region after the final crack has formed (figure 9c).

9. Discussion of Design Choices

The aim of this work is to provide material engineers with methods for 4DCT visualization and analysis. We organized the design and development process in the following way. First, together with material engineers, we formalized their requirements and needs into a set of tasks (provided in section 2). Then, in a series of discussions, we defined the methods that would be prototyped. Each idea for a new method was ranked based on two criteria: 1) the ability of the

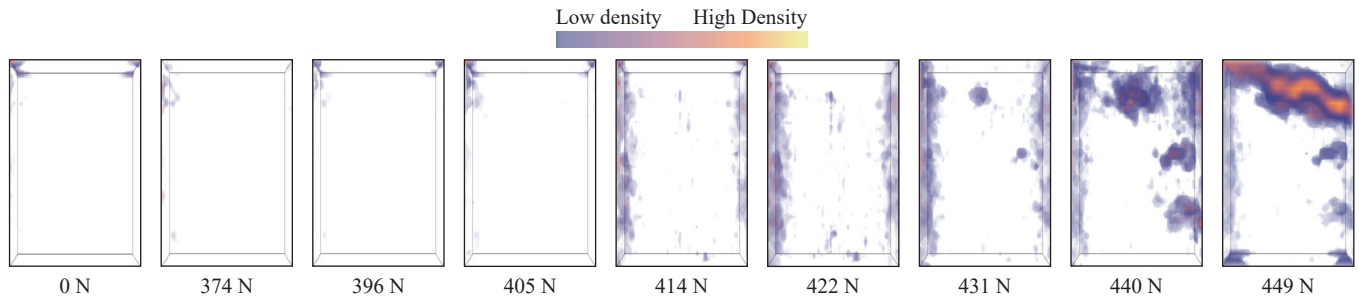


Figure 11: A series of Defect Density Maps showing the defect development process from the first to the last stage for the Dataset 3. Direct volume rendering is used. A color transfer function is shown on the top.

suggested method to solve its analysis tasks, and 2) the cost of implementing the method. Ideas with the highest rankings were then prototyped. Finally, the prototypes were presented to the material engineers. Using their feedback, we picked a set of methods for the final implementation.

We chose to implement the **Defect Viewer** and the **Defect Density Maps** because they have relatively low implementation complexities and were considered sufficient for solving tasks of the material engineers. For the Final Fracture Surface and the 3D Magic Lens, a few alternatives were discussed.

Final Fracture: At early prototyping stages, we considered the alternative of representing the final fracture as a 3D volume. When implementing this approach we encountered two main issues:

- After the fracture appears, its thickness keeps changing in the following steps but the fracture surface shape remains the same. This hinders the comparative analysis between late tensile-test stages.
- Since defects could occur in the whole volume of the specimen, it is not clear where the border of the final fracture should be defined. To resolve this issue, the density parameter could be used, which leads to an additional complexity of the final fracture extraction algorithm. In the end, it would make the comparison of two fractures a non-trivial task.

Based on the above considerations, the approach of representing the final fracture as a surface in 3D proved to be more suitable for our analysis tasks (see figure 8).

3D Magic Lens: As alternative comparative visualization methods, we considered side-by-side and checkerboard image displays. For the latter, the checkerboard pattern is used where black squares show one image and white squares show the other image. We chose the 3D Magic Lens because of the following reasons:

- The interactive functions of the 3D Magic Lens were rated as highly useful by the material engineers.
- The resulting visualization was considered easier to interpret.
- Due to its local nature, the 3D Magic Lens enabled the user to focus only on important changes and only on the regions where they are relevant.
- When the checkerboard visualization was used, borders between two squares could go through an important feature, like defect or fiber. The 3D Magic Lens visualization avoids such cases.

10. Conclusions and Future Work

We have presented a workflow for the visual analysis of 4DCT data. The workflow comprises two parts: 1) defect extraction and classification, and 2) visual analysis. A novel defect classification method based on commonly accepted domain-specific criteria is introduced. Four approaches for the interactive visual analysis of 4DCT data are presented and evaluated, i.e., Defect Viewer, Defect Density Maps, Final Fracture Surface, and 3D Magic Lens. The methods complement each other and can be combined for more flexible visualizations tailored to specific analysis tasks. The presented methods were continuously evaluated in close feedback loops with industry and university material engineers, all of whom work with GFRPs on a daily basis. Further evaluation interviews resulted in positive feedback and confirm the importance of these methods in the area of 4DCT tensile tests. In future work, we will focus on applying these tools to other materials. Currently, carbon fiber reinforced polymers and natural fiber reinforced polymers are interesting for industry as well. In addition, particular attention will be given to finding correlations between fractures and material properties. An extensive base of defects should be compiled and used to predict fractures in new materials. Future work also includes the studying of methods for a non-rigid registration or morphing of the interrupted *in situ* tensile test stages. This would allow material engineers to navigate between the stages and visualize the continuous development of defects and fractures either by using animations or by highlighting the regions where the largest deformation occurs.

11. Acknowledgments

This work was supported by funding from the European Union's Seventh Framework Programme (FP7/2007-2013) under grant agreement PITN-GA-2013-607817-INTERAQCT and has also partly received funding from the FFG Bridge Early Stage project no. 851249, BF: Advanced multimodal data analysis and visualization of composites based on grating interferometer micro-CT data (ADAM). We wish to thank our company partner Borealis AG for their helpful feedback. We also thank Massimiliano Ferrucci for his valuable comments on the manuscript.

References

- [Avi] Avizo 3d software. <http://www.fei.com/software/avizo3d/>. Accessed: 2016-03-07. 2
- [BMH*14] BHOWMIK U., MANDALA D., HUDYMA N., KREIDL O., HARRIS A.: Segmentation of cracks in X-ray CT images of tested macroporous plaster specimens. In *SOUTHEASTCON 2014, IEEE* (March 2014), pp. 1–8. 4
- [FHG*09] FRITZ L., HADWIGER M., GEIER G., PITTINO G., GRÖLLER M. E.: A Visual Approach to Efficient Analysis and Quantification of Ductile Iron and Reinforced Sprayed Concrete. *IEEE TVCG* 15, 6 (October 2009), 1343–1350. 3
- [FRI89] FRIEDRICH K.: Chapter 11 - fractographic analysis of polymer composites. In *Application of Fracture Mechanics to Composite Materials*, Friedrich K., (Ed.), vol. 6 of *Composite Materials Series*. Elsevier, 1989, pp. 425 – 487. 2
- [Gra06] GRADY L.: Random walks for image segmentation. *Pattern Analysis and Machine Intelligence, IEEE Transactions on* 28, 11 (Nov 2006), 1768–1783. 4
- [HHN00] HAVRE S., HETZLER B., NOWELL L.: Themeriver: visualizing theme changes over time. In *Information Visualization, 2000. InfoVis 2000. IEEE Symposium on* (2000), pp. 115–123. 3
- [HKG07] HEINZL C., KASTNER J., GRÖLLER M. E.: *Surface Extraction from Multi-Material Components for Metrology using Dual Energy CT*. Tech. Rep. TR-186-2-07-06, Institute of Computer Graphics and Algorithms, Vienna University of Technology, Favoritenstrasse 9-11/186, A-1040 Vienna, Austria, May 2007. human contact: technical-report@cg.tuwien.ac.at. 3
- [HLRS*08] HADWIGER M., LAURA F., REZK-SALAMA C., HÖLLT T., GEIER G., PABEL T.: Interactive volume exploration for feature detection and quantification in industrial ct data. *Visualization and Computer Graphics, IEEE Transactions on* 14, 6 (Nov 2008), 1507–1514. 3
- [HMMW03] HUANG R., MA K.-L., MCCORMICK P., WARD W.: Visualizing Industrial CT Volume Data for Nondestructive Testing Applications. In *IEEE Visualization 2003 Conference* (October 2003), pp. 547–554. 3
- [ITK] The insight segmentation and registration toolkit. www.itk.org. Accessed: 2016-03-07. 4
- [LT12] LANDSTROM A., THURLEY M.: Morphology-based crack detection for steel slabs. *Selected Topics in Signal Processing, IEEE Journal of* 6, 7 (Nov 2012), 866–875. 3
- [Ots79] OTSU N.: A threshold selection method from gray level histograms. *IEEE Trans. Systems, Man and Cybernetics* 9 (1979), 62–66. 4
- [PBP*15] PAETSCH O., BAUM D., PROHASKA S., EHRIG K., MEINEL D., EBELL G.: 3D Corrosion Detection in Time-dependent CT Images of Concrete. In *Digital Industrial Radiology and Computed Tomography* (June 2015). 4
- [RAK*15] REH A., AMIRKHANOV A., KASTNER J., GRÖLLER E., HEINZL C.: Fuzzy feature tracking: Visual analysis of industrial 4d-xct data. *Computers & Graphics* 53, Part B (2015), 177 – 184. 4
- [RGK*13] REH A., GUSENBAUER C., KASTNER J., GRÖLLER M. E., HEINZL C.: Mobjects - a novel method for the visualization and interactive exploration of defects in industrial xct data. *Visualization and Computer Graphics, IEEE Transactions on* 19, 12 (Dec. 2013), 2906–2915. 3
- [RSR15] ROLLAND H., SAINTIER N., ROBERT G.: Fatigue Mechanisms Description in Short Glass Fibre Reinforced Thermoplastic By Microtomographic Observations. In *Proc. 20th International Conference on Composite Materials* (2015), Thomsen O. T., (Ed.). 5
- [SKK*11] SALABERGER D., KANNAPPAN K. A., KASTNER J., REUSSNER J., AUINGER T.: Evaluation of Computed Tomography Data from Fibre Reinforced Polymers to Determine Fibre Length Distribution. *International Polymer Processing* 26, 3 (July 2011), 283–291. 3, 4
- [SW97] SILVER D., WANG X.: Tracking and visualizing turbulent 3d features. *Visualization and Computer Graphics, IEEE Transactions on* 3, 2 (Apr 1997), 129–141. 3
- [VGS] VGStudio Max: basic functionality. <http://www.volumegraphics.com/en/products/vgstudio-max/basic-functionality/>. Accessed: 2016-03-07. 2
- [vPOBB*10] VAN PELT R., OLIVAN BESCOS J., BREEUWER M., CLOUGH R., GRÖLLER E., TER HAAR ROMENIJ B., VILANOVA A.: Exploration of 4d mri blood flow using stylistic visualization. *Visualization and Computer Graphics, IEEE Transactions on* 16, 6 (Nov 2010), 1339–1347. 3
- [WAL*14] WEISSENBOCK J., AMIRKHANOV A., LI W., REH A., AMIRKHANOV A., GRÖLLER M. E., KASTNER J., HEINZL C.: Fiberscout: An interactive tool for exploring and analyzing fiber reinforced polymers. In *Proceedings of 2014 IEEE Pacific Visualization Symposium (PacificVis)* (2014) (Mar. 2014), IEEE Computer Society, pp. 153–160. 3
- [WCBP12] WIDANAGAMAACHCHI W., CHRISTENSEN C., BREMER P.-T., PASCUCCI V.: Interactive exploration of large-scale time-varying data using dynamic tracking graphs. In *Large Data Analysis and Visualization (LDAV), 2012 IEEE Symposium on* (Oct 2012), pp. 9–17. 4
- [YNH08] YAMAGUCHI T., NAKAMURA S., HASHIMOTO S.: An efficient crack detection method using percolation-based image processing. In *Industrial Electronics and Applications, 2008. ICIEA 2008. 3rd IEEE Conference on* (June 2008), pp. 1875–1880. 4
- [ZYZ10] ZHOU H., YANG S., ZHU J.: Illumination Invariant Enhancement and Threshold Segmentation Algorithm for Asphalt Pavement Crack Image. In *Wireless Communications Networking and Mobile Computing (WiCOM), 2010 6th International Conference on* (Sept 2010), pp. 1–4. 3